Crystal Structures of Branched-Chain Amino Acid Aminotransferase Complexed with Glutamate and Glutarate: True Reaction Intermediate and Double Substrate Recognition of the Enzyme[†,‡]

Masaru Goto,[§] Ikuko Miyahara,[§] Hideyuki Hayashi,[⊥] Hiroyuki Kagamiyama,[⊥] and Ken Hirotsu*[,§]

Department of Chemistry, Graduate School of Science, Osaka City University, Sugimoto, Sumiyoshi-ku, Osaka 558-8585 Japan, and Department of Biochemistry, Osaka Medical College, Takatsuki, Osaka 569-8686 Japan

Received August 24, 2002; Revised Manuscript Received November 30, 2002

ABSTRACT: Branched-chain amino acid aminotransferase (BCAT), which has pyridoxal 5′-phosphate as a cofactor, is a key enzyme in the biosynthetic pathway of hydrophobic amino acids (leucine, isoleucine, and valine). The enzyme reversibly catalyzes the transfer of the amino group of a hydrophobic amino acid to 2-oxoglutarate to form a 2-oxo acid and glutamate. Therefore, the active site of BCAT should have a mechanism to enable recognition of an acidic amino acid as well as a hydrophobic amino acid (double substrate recognition). The three-dimensional structures of *Escherichia coli* BCAT (eBCAT) in complex with the acidic substrate (glutamate) and the acidic substrate analogue (glutarate) have been determined by X-ray diffraction at 1.82 and 2.15 Å resolution, respectively. The enzyme is a homo hexamer, with the polypeptide chain of the subunit folded into small and large domains, and an interdomain loop. The eBCAT in complex with the natural substrate, glutamate, was assigned as a ketimine as the most probable form based upon absorption spectra of the crystal complex and the shape of the residual electron density corresponding to the cofactor−glutamate bond structure. Upon binding of an acidic substrate, the interdomain loop approaches the substrate to shield it from the solvent region, as observed in the complex with a hydrophobic substrate. Both the acidic and the hydrophobic side chains of the substrates are bound to almost the same position in the pocket of the enzyme and are identical in structure. The inner side of the pocket is mostly hydrophobic to accommodate the hydrophobic side chain but has four sites to coordinate with the γ-carboxylate of glutamate. The mechanism for the double substrate recognition observed in eBCAT is in contrast to those in aromatic amino acid and histidinol-phosphate aminotransferases. In an aromatic amino acid aminotransferase, the acidic side chain is located at the same position as that for the aromatic side chain because of large-scale rearrangements of the hydrogen bond network. In the histidinol-phosphate aminotransferase, the acidic and basic side chains are located at different sites and interact with different residues of the disordered loop.

Aminotransferases, which are pyridoxal 5′-phosphate (PLP[1])-dependent enzymes, reversibly catalyze a transamination reaction, which consists of essentially the same two half reactions (Scheme 1) (*1*). The α-amino group of amino acid 1 is transferred to the PLP to give a pyridoxamine 5′-phosphate (PMP) and 2-oxo acid of the amino acid. Next, 2-oxoglutarate accepts the amino group of PMP to yield glutamate and regenerate PLP.

Scheme 1

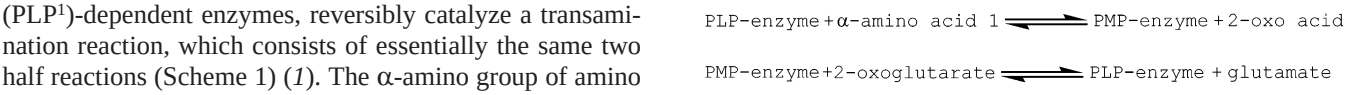

Usually, an aminotransferase has its own α-amino acid (or amine) as the substrate in one of two half reactions and a common amino acid, glutamate, in the other (Scheme 1). For example, an aromatic amino acid aminotransferase accepts aromatic amino acids as amino acid 1. Two kinds of amino acids, the side chains of which are different in shape and properties, can be recognized from many other small molecules by the sophisticated design of the active site in comparison with single substrate recognition. The mechanism for the double substrate recognition in aromatic amino acid and histidinol-phosphate aminotransferases has been clarified by X-ray crystallographic studies (*2-4*). In an aromatic amino acid aminotransferase, both acidic and aromatic side chains of the substrate are bound to the pockets formed at the same location of the active site because of a rearrangement of the hydrogen bond network of the active site without a confor-

[†] This study was supported in part by the following grants: Grant-in-aid for Scientific Research on Priority Area from the Ministry of Education, Science, Sports, and Culture of Japan [B: 13125207 (K.H.)], Research Grant from the Japan Society for the Promotion of Science [Category B: 13480196 (K.H.)], and National Project on Protein Structural and Functional Analyses.

[‡] Coordinates for eBCAT complexes with glutarate and glutamate have been deposited in the RSCB Protein Data Bank as entry 1IYD and 1IYE, respectively.

* To whom correspondence should be addressed. E-mail: hirotsu@sci.osaka-cu.ac.jp. Fax: +81-6-6605-3131.

[§] Osaka City University.

[⊥] Osaka Medical College.

[1] Abbreviations: PLP, pyridoxal 5′-phosphate; PMP, pyridoxamine 5′-phosphate; BCAT, branched-chain amino acid aminotransferase; eBCAT, *Escherichia coli* BCAT; hmBCAT, human mitochondrial BCAT; bsDAAT, *Bacillus* sp. YM-1 D-amino acid aminotransferase; rms, root-mean-square; Tyr31*, the asterisk (*) indicates a residue from another subunit of the dimer unit.

10.1021/bi026722f CCC: $25.00
Published on Web 03/15/2003

Scheme 2

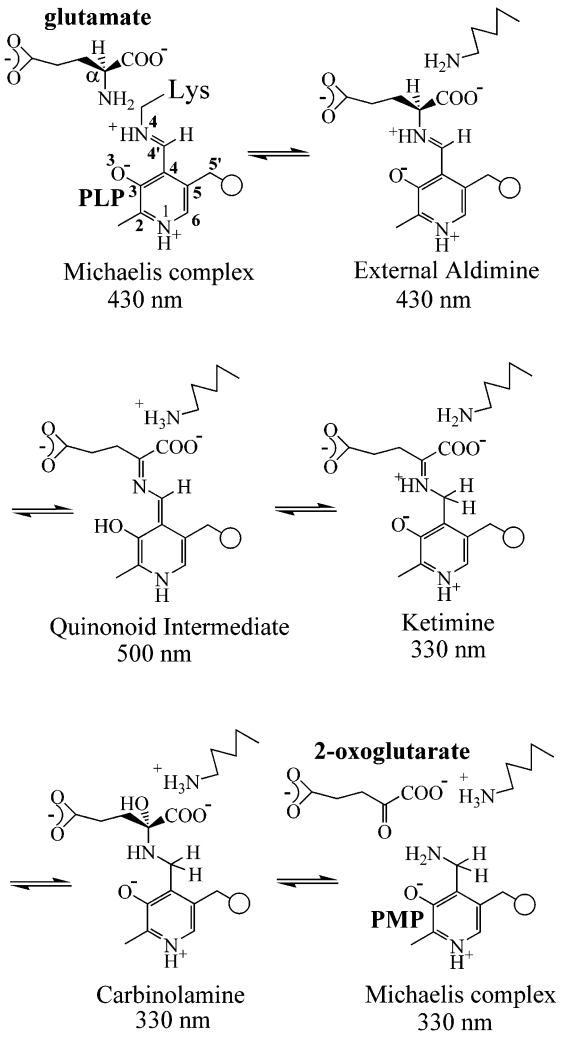

mational change in the backbone structure of the enzymes (*2*, *3*). In contrast, histidinol-phosphate aminotransferase recognizes the basic side chain of histidinol phosphate and the acidic side chain of glutamate at different positions of the active site by an induced fit mechanism utilizing the flexible loop of the enzyme (*4*).

Most of the PLP-dependent enzymes are classified into four distinct fold types (*5*, *6*). The fold type IV enzyme is characterized by proton transfer on the *re*-face of PLP, in contrast to the *si*-face specificity of proton transfer in the enzymes of other fold types (*7-12*, *14*). The branched-chain amino acid aminotransferase (BCAT) belongs to the fold type IV and is specific for hydrophobic amino acids (L-isoleucine, L-leucine, and L-valine) and L-glutamate (*15*). Thus, BCAT has the capability to recognize not only a hydrophobic side chain but also an acidic side chain. The BCAT from *Escherichia coli* (eBCAT) is a homo hexamer, which is an assembly of three dimer units around a 3-fold axis. Each subunit consists of 308 amino acid residues with a molecular weight of 31 500 Da and contains a bound PLP as a cofactor.

The eBCAT catalyzes a reversible transamination reaction between the hydrophobic amino and the α-keto acids. The reaction of eBCAT with glutamate proceeds from a Michaelis complex in PLP form through an external aldimine, a quinonoid intermediate, a ketimine, and a carbinolamine to a Michaelis complex in PMP form as shown in Scheme 2 (*16*, *17*). In the case of a reversible reaction, a thermodynamically stable form of the enzyme might accumulate resulting in the X-ray structure determination of the true intermediate. In fact, the structures of the enzyme substrate complexes have been reported for aspartate and histidinol-phosphate aminotransferases (*4*, *18*).

Although the structures of eBCAT complexes with hydrophobic substrate analogues (2-methylleucine and 4-methylvalerate) have been determined (*11*), the interaction of eBCAT with an acidic substrate has not yet been investigated. The eBCAT complexed with glutamate or its analogue should aid in understanding the mechanism for enzyme−substrate binding in aminotransferases, by comparing the double substrate recognition of eBCAT with that of an aromatic amino acid or histidinol-phosphate aminotransferase. The X-ray analysis of eBCAT•glutamate is the first structural elucidation of a true intermediate in a fold type IV enzyme giving the structural basis for catalytic action. We now report the X-ray crystallographic studies of eBCAT•glutamate as ketimine and eBCAT•glutarate as a Michaelis complex model at 1.82 and 2.15 Å resolution, respectively.

MATERIALS AND METHODS

Crystallization and Data Collection. All chemicals were of the highest purity available from commercial sources. The expression of eBCAT, the purification of the expressed enzyme, and the crystallization of the purified enzyme have been reported elsewhere (*10*, *11*, *15*). Briefly, the eBCAT in complex with the true substrate glutamate was crystallized using 40 mg/mL protein solution and 42% (v/v) PEG400, 200 mM $MgCl_2$, 50 mM glutamate, 100 mM Na-HEPES, pH 7.5, as the reservoir solution to yield colorless crystals. The eBCAT in complex with glutarate was crystallized using the same procedure as that for the glutamate complex except that 50% (v/v) PEG400 and 100 mM glutarate were used instead of 50 mM glutamate to yield yellow crystals.

The X-ray diffraction data sets for the eBCAT•glutamate and eBCAT•glutarate crystals were collected to 1.82 and 2.15 Å resolution at 100 K on the BL41XU station at SPring-8 (Hyogo, Japan), respectively. Both crystals belonged to space group $C222_1$ and had the following cell dimensions: a = 154.6, b = 98.9, and c = 138.8 Å for eBCAT•glutamate and a = 154.3, b = 99.0, and c = 138.6 Å for eBCAT•glutarate. There are three subunits in the asymmetric unit, and approximately 54% of the crystal volume is occupied by solvent. All data were processed and scaled using the programs DENZO and SCALEPACK (*19*) (Table 1).

Structure Determination. The initial phases computed from the structure of the unliganded form, except for the PLP cofactors and solvents (*10*), were applied to the diffraction data between 10 and 2.4 Å for both complexes, resulting in an R_{factor} of 0.36 for eBCAT•glutamate and 0.34 for eBCAT•glutarate. Difference Fourier maps of the active sites were calculated, and the large electron densities were assigned to the cofactor, glutarate, and glutamate (Figure 1) (*20*).

In the eBCAT•glutamate, the spectra of the colorless crystal showed a loss of absorption at 430 nm and a new absorption band at 330 nm (Figure 2). Thus, the glutamate complex should be one of ketimine, carbinolamine, and the PMP•2-oxoglutarate forms shown in Scheme 2. The residual

Table 1: Data Collection and Refinement Statistics

crystal	ketimine	glutarate
data collection		
resolution (Å)	1.82	2.15
no. of reflections		
unique	92 593	58 165
observed	534 649	324 820
completeness (%)	97.5 (99.8)[a]	99.5 (96.8)[a]
R_{merge} (%)[b]	5.5 (16.7)[a]	7.0 (19.5)[a]
refinement		
resolution limits (Å)	19.96−1.82	19.96−2.15
R_{factor} (%)	20.9 (26.3)[a]	20.5 (25.9)[a]
R_{free} (%)	23.9 (30.1)[a]	24.2 (30.6)[a]
deviations		
bond lengths (Å)	0.006	0.007
bond angles (deg)	1.35	1.35
mean B factors		
main-chain atoms (Å^2)	19.8	23.9
side-chain atoms (Å^2)	22.0	25.8
heteroatoms (Å^2)	19.0	24.4
water atoms (Å^2)	25.7	24.9

[a] The values in the parentheses are for highest resolution shells (1.89−1.82 Å) in the glutamate complex and (2.22−2.15 Å) in the glutarate complex. [b] $R_{merge} = \sum_{hkl}\sum_i|I_{hkl,i} - \langle I_{hkl}\rangle|/\sum_{hkl}\sum_i I_{hkl,i}$, where I = observed intensity and $\langle I\rangle$ = average intensity for multiple measurements.

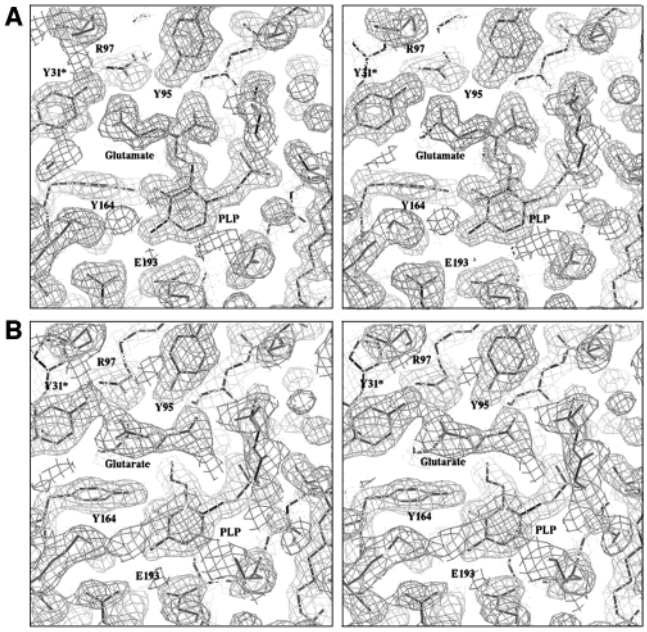

FIGURE 1: (A) Stereoview of the $2F_o - F_c$ electron density map calculated using data between 8.0 and 1.82 Å resolution for eBCAT•glutamate. The electron density map shows the formation of a covalent bond between glutamate and cofactor. (B) Stereoview of the $2F_o - F_c$ electron density map calculated using data between 8.0 and 2.15 Å resolution for eBCAT•glutarate.

electron density of glutamate is connected to the C4′ atom of the cofactor, indicating that glutamate is covalently bound to the cofactor. The glutamate−cofactor bond structure was thus assumed to be ketimine or carbinolamine. The ketimine form showed a good fit to the electron density, but the α-OH group of carbinolamine could not be fitted into the electron density. Therefore, the glutamate−cofactor bond structure was assigned to be ketimine as the most probable form.

The missing region (Gly127-Glu133) of the interdomain loop in the unliganded form was distinctly located on a $F_o - F_c$ map of eBCAT•glutamate and eBCAT•glutarate. The water molecules that had thermal factors above 50 Å^2 after refinement were removed from the list. Model building and refinement cycles resulted in an R_{factor} of 0.209 and R_{free} of 0.239 using 92 560 reflections [$F_o > 2\sigma(F_o)$] between 20 and 1.82 Å resolution for the eBCAT•glutamate complex and in an R_{factor} of 0.205 and R_{free} of 0.242 using 56 634 reflections [$F_o > 2\sigma(F_o)$] between 20 and 2.15 Å resolution for the eBCAT•glutarate complex (*21*) (Table 1).

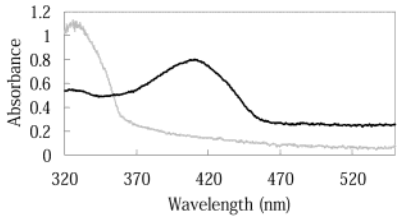

FIGURE 2: Absorption spectra of eBCAT crystal in the absence (thick line) and the presence (thin line) of substrate glutamate at pH 7.5 and 100 K.

Spectrophotometric Measurements. The crystal absorption spectra of the native eBCAT and eBCAT in complex with glutamate were recorded with a spectrophotometer at 100 K in the laboratory of the Division of Bio-crystallography Technology (RIKEN Harima Institute, Hyogo, Japan). These were normalized by the crystal thickness. The free enzyme exhibited a 430 nm absorption band characteristic of the internal aldimine form of the enzyme. The enzyme in complex with glutamate exhibited a new absorption band at 330 nm with the disappearance of the 430 nm absorption (Figure 2).

Quality of the Structures. The final models for the two complexes comprise 3 × 304 residues (three N-terminal residues and one C-terminal residue of each subunit were not visible), three PLPs, and 500 water molecules for eBCAT•glutamate and 311 water molecules for eBCAT•glutarate. The main-chain atoms of the three subunits in the asymmetric unit were superimposed using the least-squares method fitting with an rms deviation of 0.25 and 0.25 Å with a maximum deviation of 1.29 and 1.05 Å for eBCAT•glutamate and eBCAT•glutarate, respectively. This result indicates that the overall structures of the three independent subunits are quite similar. The average thermal factors of the main-chain atoms (N, Cα, C, O) in the three subunits are 20.3, 20.3, and 15.8 Å^2 for eBCAT•glutamate and 25.7, 25.7, and 20.3 Å^2 for eBCAT•glutarate.

Analysis of the stereochemistry with PROCHECK (*22*) showed that all the main-chain atoms except for Glu260 fall within the generously allowed regions of the Ramachandran plot for the eBCAT•glutamate and the eBCAT•glutarate complexes. On the basis of the electron density maps, it was confirmed that the conformations of Glu260 were correct. Structure diagrams were drawn with the programs Molscript (*23*), Bobscript (*24*), and Raster3D (*25*).

RESULTS AND DISCUSSION

Overall Structure. The overall structures of the eBCAT•glutamate and the eBCAT•glutarate complexes are quite similar to those of eBCAT•4-methylvalerate or that of eBCAT•2-methylleucine (*11*). The enzyme is a homo hexamer (a trimer of dimers). The subunit structure of eBCAT•glutamate is shown in Figure 2. The overall structure of the subunit is essentially the same as those of bsDAAT (*8, 9*) and *E. coli* 4-amino-4-deoxychorismate (*14*), which also belong to the

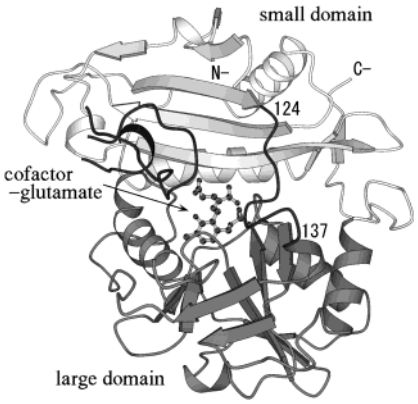

FIGURE 3: View of the subunit structure in eBCAT in complex with glutamate. The shaded and open ribbons represent the large and the small domains, respectively. The interdomain loop and the loops from the other subunit of the dimer unit are shown by the full ribbons. The cofactor−glutamate bond structure is drawn by the ball-and-stick model.

fold type IV group. The polypeptide chain of the subunit is folded into the small domain (N-terminal to Tyr124 and Leu-303 to Gln308) characterized by the α/β structure, the interdomain loop (Pro125 to Glu136), and the large domain (Gln-137 to Trp302) characterized by a pseudo barrel structure. The cofactor and the substrate glutamate are bound to the bottom of the active site cavity between the small and the large domains of one subunit and two loops from the small domain of the other subunit form one side of the active site. Thus, the active site comprises residues from both domains of one subunit and the small domain of the other subunit. The interdomain loop, which is disordered in the unliganded form of eBCAT (*11*), has an ordered structure that approaches the substrate and hangs over the active site entrance.

Active Site of eBCAT•Glutamate as the True Ketimine Intermediate. The active site structures of the unliganded eBCAT and eBCAT•glutamate are shown in Figure 4A,B, respectively. The hydrogen-bonding scheme of the active site in eBCAT•glutamate is displayed in Figure 5. In the reversible reaction of an enzyme, there is a possibility that the thermodynamically stable intermediate is captured using crystals obtained by soaking the native crystals in solutions containing the substrates (*18*) or by cocrystallizing the enzyme with the substrates (*4*). The eBCAT was cocrystallized with an excess of the substrate glutamate to yield crystals of a true intermediate complex. The major component of the glutamate−cofactor bond structure was assigned to be ketimine based on the spectra of the crystal and the agreement between the substrate model and the residual electron density (see Materials and Methods). The eBCAT•glutamate presents an excellent model of the complex structure free from the bias caused by structural differences between substrate analogues (or inhibitors) and the true substrates.

Upon binding with glutamate, Arg40, Tyr164, and the interdomain loop significantly change their arrangements, while other residues retain their locations because the residues of eBCAT•glutamate fit the corresponding residues in the unliganded eBCAT with an rms deviation of 0.2 Å and a maximum displacement of 0.9 Å when Arg40, Tyr164, and the interdomain loop are neglected (Figure 4A,B). The binding of glutamate liberates two out of five water molecules located in the active site of the unliganded enzyme (*10*, *11*). The interdomain loop, which is disordered in the unliganded form, displays an ordered structure as the lid of the active site and shields the glutamate from the solvent region. The glutamate binding induces a directional change of Arg40 from the solvent side to the active site region. The guanidino group of glutamate interacts with the main chain carbonyl groups of Thr257 and Ala258 of the β-turn and with those of Trp126 and Gly127 of the interdomain loop as observed in eBCAT•4-methylvalerate or eBCAT•2-methylleucine (Figures 4B and 5). Arg40 may play an important role in the induced fit of the interdomain loop by bridging the β-turn and the interdomain loop. The cofactor forms a new covalent bond with the glutamate in place of the catalytic residue Lys159. The released amino group of Lys159, which shuttles protons on the *re*-face side of the cofactor, forms hydrogen bonds with the hydroxy group of Tyr164 and O3- of the cofactor, which would decrease the free energy level of the eBCAT•glutamate complex in the ketimine form. In the aspartate and ornithine aminotransferases (*26*−*34*), tyrosine and threonine take the place of Tyr164, respectively, which are on the phosphate group side of PLP. One of the α-carboxylate oxygen atoms of glutamate forms a hydrogen bond with the hydroxyl group of Tyr95, and the other is involved in three hydrogen bonds with the main-chain NH groups of Thr257 and Ala258 at the β-turn and with W3. One of the γ-carboxylate oxygen atoms of glutamate interacts with the guanidino group of Arg97 and the hydroxy group of Tyr31*, and the other is hydrogen bonded to the hydroxyl group of Tyr129 of the interdomain loop and the main-chain NH group of Val109*.

The pyridine ring of PLP rotates by about 28° around the N1−C6 bond toward the solvent side as compared with that in the unliganded enzyme to form a direct bond with the glutamate located on the *si*-face of the cofactor. The 30° rotation of the PLP ring around the N1−C6 bond was also observed in eBCAT•2-methylleucine as the external aldimine model. The torsional angle of C3−C4−C4′−N of the cofactor−glutamate bond structure is 43° (30° in eBCAT•2-methylleucine). The rotation of the PLP ring allows the approach of the O3- of PLP to the hydroxy group of Tyr164 to induce a fairly large movement of the side chain of Tyr164 (*11*). The side chain of Tyr164 moves from the *si*-face side of the cofactor to the *re*-face side to maintain the hydrogen bond with O3-. As a result of this, the hydroxy group of Tyr164 interacts with the released Lys159.

Active Site of the eBCAT•Glutarate as a Michaelis Complex Model. The active site structure of eBCAT•glutarate is shown in Figure 4C. The glutarate is a substrate analogue where the α-amino group of glutamate is replaced by a hydrogen atom. The location and conformation of the PLP−Schiff base are quite similar to those in eBCAT•4-methylvalerate. The torsional angle of C3−C4−C4′−N in the PLP−Schiff base bond is −13° (4° in eBCAT•4-methylvalerate), which shows that the internal aldimine bond (Schiff base, C4′ = N) is essentially coplanar with the PLP ring to form a PLP−Schiff base conjugate system. The substrate analogue glutarate is located on the *si*-face of PLP with one of the Cα hydrogen atoms of glutarate directed toward C4′ of the Schiff base in PLP. The α- and γ-carboxylates of the glutarate occupy positions similar to the corresponding groups of the glutamate in the ketimine intermediate, forming

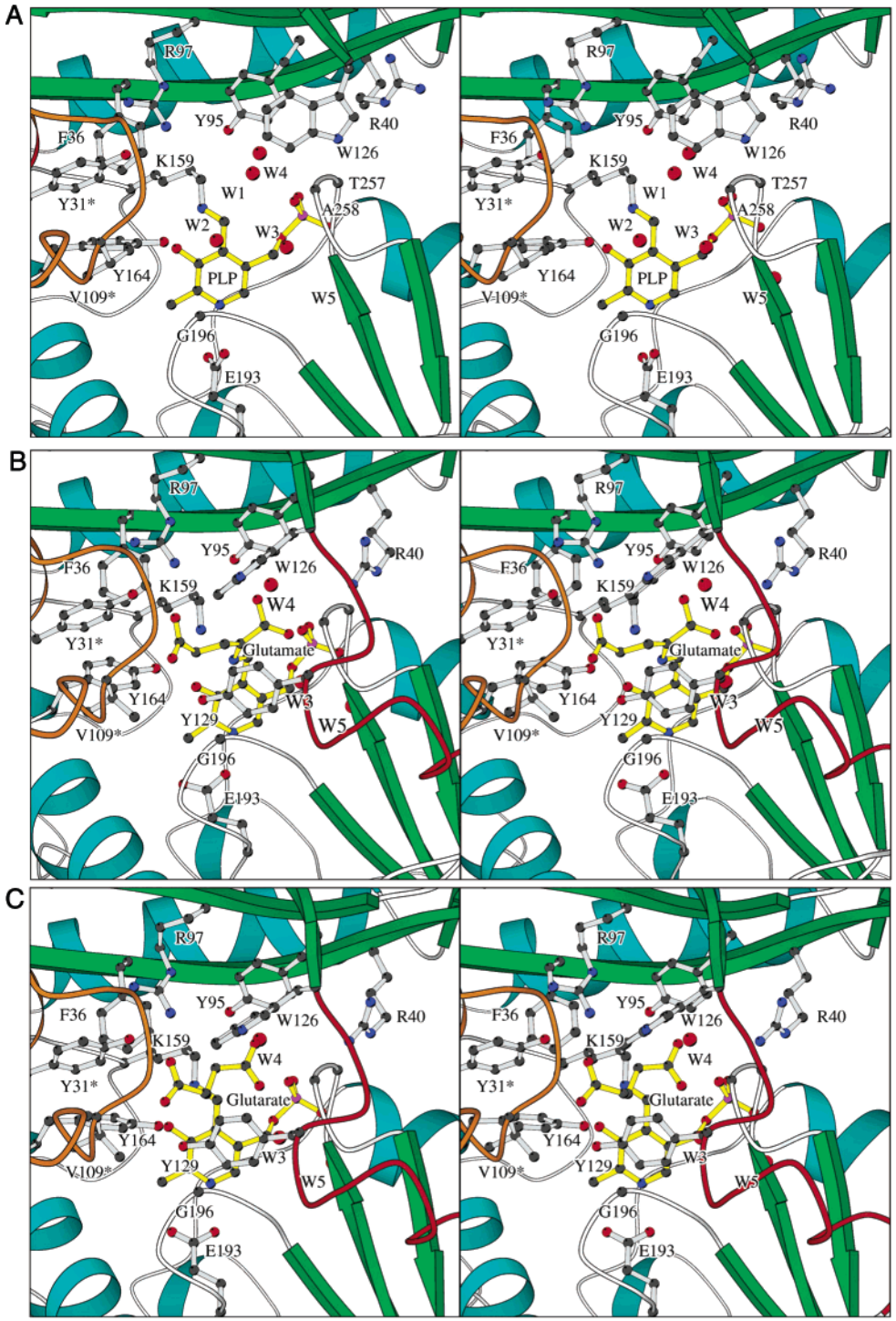

FIGURE 4: Stereoview of the active site in eBCAT. The front and back of each figure are the solvent side (entrance of the active site) and the protein side (bottom of the active site), respectively. (A) A close-up view of the active site of the unliganded eBCAT. The loops (orange) carrying Y31* and V109* of the small domain of the other subunit participate in the formation of the active site. The active site residues and PLP (yellow) are shown by a ball-and-stick model. The interdomain loop is missing because the region is disordered. (B) A close-up view of the active site of eBCAT in complex with glutamate. The missing interdomain loop in the unliganded form showed its ordered structure (red) on the active site and is displayed with Trp126 and Tyr129. The cofactor and glutamate bond structure is colored yellow. Omit electron density map is contoured at a 1.0 σ level. (C) A close-up view of the active site of the eBCAT in complex with glutarate. The glutarate and the cofactor are yellow. Omit electron density map is contoured at a 1.0 σ level.

hydrogen bonds with the neighboring residues in the same manner as observed in eBCAT•glutamate.

The active site residues of eBCAT•glutarate fit the corresponding residues in the unliganded eBCAT with an rms deviation of 0.4 Å when Arg40 and the interdomain loop are not included. The rms deviation of the active site residues between eBCAT•glutarate and eBCAT•glutamate is 0.5 Å except for Tyr164, indicating that the active site structure surrounding the cofactor and the substrate (or the analogue) is quite similar in both complexes (Figure 6A). The superposition of the active site residues between eBCAT•glutarate and eBCAT•4-methylvalerate as a Michaelis complex model and between eBCAT•glutamate and eBCAT•2-methylleucine as the cofactor−substrate adduct model are shown in Figure

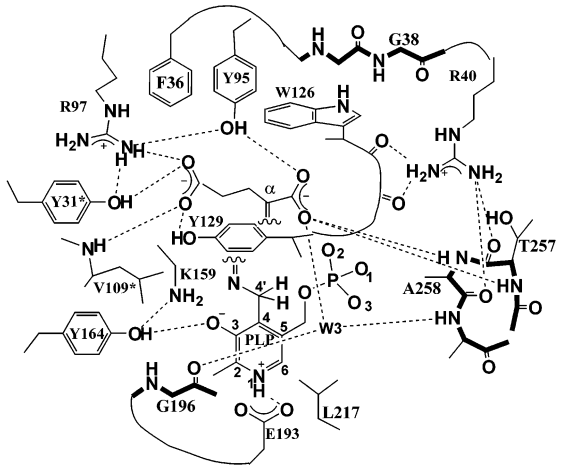

FIGURE 5: Schematic diagram showing hydrogen bond and salt bridge interactions of the active site residues in eBCAT•glutamate. The Cα=N double bond of the cofactor−glutamate adduct is broken for clarity. Putative interactions are shown by the dotted lines if the acceptor and donar are less than 3.3 Å apart. Water molecules (W4 and W5) and the hydrogen bonds associated with the phosphate group of PLP are omitted for clarity.

6B,C, respectively. The main-chain folding and the side-chain arrangement of the active site residues are essentially the same among eBCAT complexes with glutarate, glutamate, 4-methylvalerate, and 2-methylleucine, although the side chains of Tyr129, Tyr164, and Val109* show significant deviations. This is because the corresponding residues are superimposed by a least-squares method among these complexes with an rms deviation of 0.4−0.5 Å.

Double Substrate Recognition. The eBCAT recognizes the hydrophobic amino acids and glutamate, which are different in shape and properties, using the same active site. The mechanism for the double substrate recognition in eBCAT has now been determined. On the approach of a substrate to the active site, its α-carboxylate and side chain groups bind to the phosphate side and the O3- side of the cofactor, respectively, by liberating two water molecules. The α-carboxylate of a substrate is recognized by the hydroxy group of Tyr95 polarized by the coordination of Arg97 and the main-chain NH groups of Thr257 and Ala258 at the *β*-turn. Arg40 interacts with the main-chain carbonyl groups of the *β*-turn, thus activating the main-chain NH groups on the other side (Figure 5).

The binding pocket for the side chain of a substrate amino acid is formed by Phe36, Arg97, Trp126, Tyr129, Tyr164, Tyr31*, and Val109*. The bulky side chain of a hydrophobic amino acid is encapsulated in this pocket and primarily interacts with the aromatic rings of the surrounding residues. The inner surface of the binding pocket is mostly hydrophobic but has four sites to encircle and recognize the *γ*-carboxylate of the glutamate: the guanidino group of Arg97, the hydroxy group of Tyr31*, the hydroxy group of Tyr129 from the interdomain loop, and the main-chain NH group of Val109*. The acidic side chain of the glutamate, which is longer by one methylene group than the hydrophobic side chain, can make its terminal carboxylate approach within the hydrogen bonding distances with these four polar sites (Figure 5), resulting in a fully coordinated *γ*-carboxylate: one salt bridge and three hydrogen bonds.

The double substrate recognition in an aromatic amino acid aminotransferase (*2*, *3*) and a histidinol-phosphate aminotransferase (*4*) has been elucidated. In the aromatic amino acid aminotransferase, the aromatic and acidic side chains are located at the same place of the active site but are enclosed in different surroundings by the large-scale rearrangement of the hydrogen-bond network of the active site. In the histidinol-phosphate aminotransferase, the basic and acidic side chains of histidinol phosphate are located at different recognition sites and are accessed by different residues of the disordered loop in the unliganded enzyme. The mechanism for the recognition of eBCAT is different from that of either an aromatic amino acid or a histidnol-phosphate aminotransferase. In eBCAT, the identical pocket, which is hydrophobic overall with relatively localized hydrophilic sites, can accommodate the hydrophobic and acidic side chains of the substrates at approximately the same position.

The active site structure of hmBCAT inhibited by Tris, where Tris is covalently bonded to the pyridoxal and the catalytic Lys, has been compared with that of eBCAT•glutamate (*12*). All the active site residues depicted in Figure 5 are conserved in hmBCAT except for Arg40 (Lys in hmBCAT), Gly196 (Thr), and the interdomain loop. The active site residues of eBCAT except for the residues from the interdomain loop were superimposed onto the corresponding atoms of hmBCAT with rms deviations of 0.53 Å for Cα atoms and 0.67 Å for main-chain and side-chain atoms of the conserved residues. This indicates that not only the active site folding but also the arrangements of the active site residues are quite similar between eBCAT and hmBCAT. Therefore, it is reasonable to assume that the substrates bound to the active sites of hmBCAT are recognized in a similar way as that observed in eBCAT. The primary sequence of hmBCAT is characterized by additional 39 N-terminal residues as compared with that of eBCAT. Interestingly, the phenyl ring of Phe30 belonging to the additional residues replaces the indole ring of Trp126 of the interdomain loop in eBCAT and partially covers the active site cavity. The interdomain loop of hmBCAT has an ordered structure not only in the native form but also in the complex with Tris, and its location and conformation is considerably different from that in eBCAT. Thus, the interdomain loop of hmBCAT might behave differently from that of eBCAT. However, this assertion can only be validated by the X-ray crystallographic determination of hmBCAT in complex with a substrate or a substrate analogue.

The orientation of the cofactor in bsDAAT belonging to the fold type IV enzyme is the same as that in BCAT, while the substrate bound to bsDAAT is rotated by 180° as compared with that in BCAT, indicating that the substrate α-carboxylate and side chain in bsDAAT are on the O3- and phosphate group sides of the cofactor, respectively (*8*−*11*). Most of the active site residues of bsDAAT necessary for substrate recognition are not conserved in eBCAT or hmBCAT, although the main-chain conformation is similar between them (*10*). The α-carboxylate of D-Ala bound to bsDAAT makes a salt bridge with Arg98* and interacts with Tyr31 and His100*. In eBCAT, Arg98*, Tyr31, and His100* are replaced by Met107*, Phe36, and Val109*, which are involved in the formation of the hydrophobic pocket. The side-chain methyl group of D-Ala is located in the neutral pocket formed by Val33 (Gly38 in eBCAT), Thr241 (Thr257), and Thr242 (Ala258). The pocket is relatively large and may accommodate either hydrophobic or hydrophilic

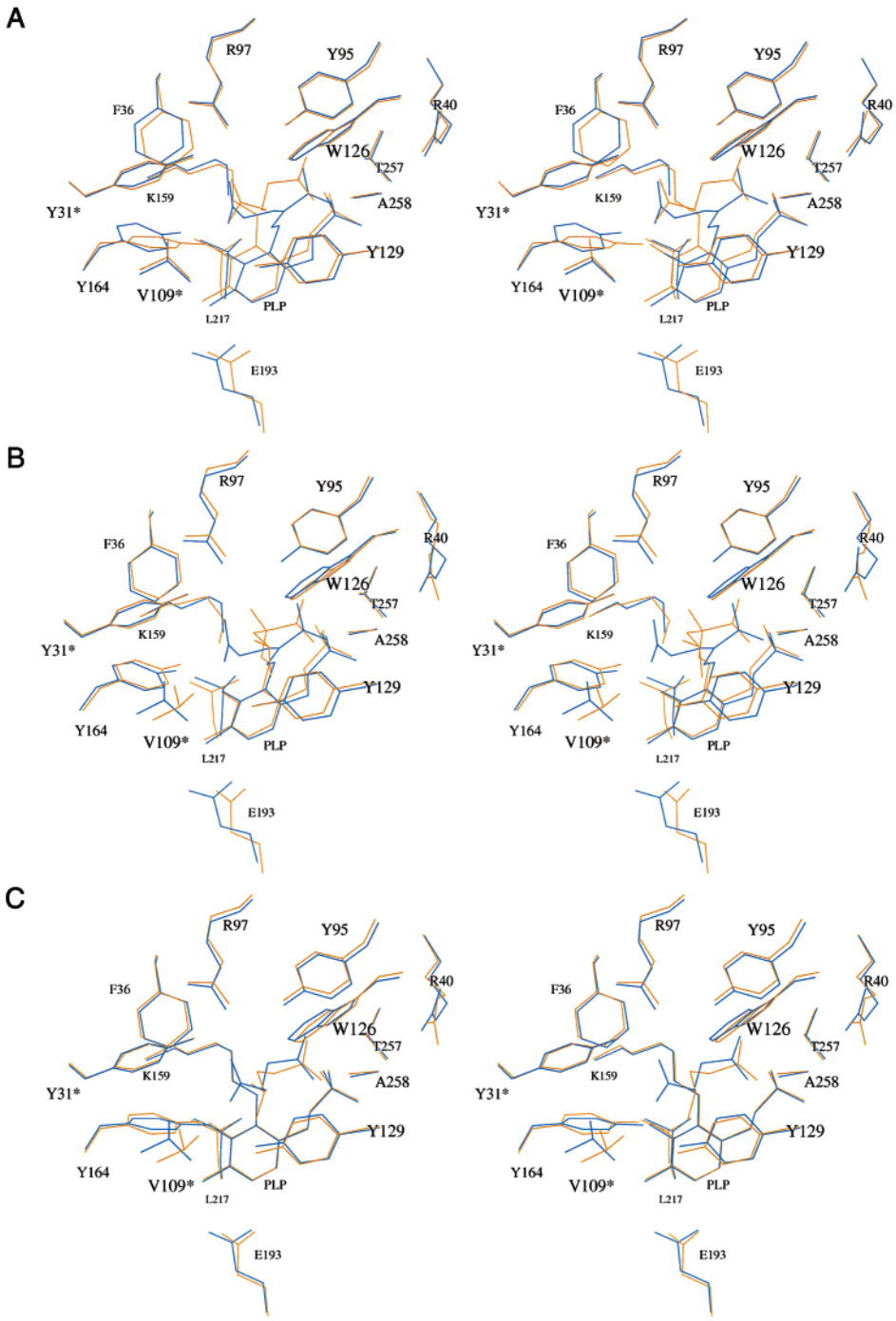

FIGURE 6: Fitting of the active site residues by least-squares except for Tyr164. (A) Superimposition between eBCAT complexes with glutamate (blue) and glutarate (yellow). The active site residues are well-overlapped except Tyr164. (B) Superimposition between eBCAT complexes with glutamate (blue) and 2-methylleucineb (yellow). (C) Superimposition between eBCAT complexes with glutarate (blue) and 4-methylvarelate (yellow).

side chains, which is consistent with the wide spectrum of substrate amino acids for bsDAAT (*35*). The change in substrate specificity from an L-amino acid to the enantiomer, a D-amino acid, can only be achieved through the replacement of active site residues, without a change in the main-chain fold of the active site (*10*, *11*)

Mechanism. On the basis of the active site structures of the unliganded form, Michaelis complex models (eBCAT complexes with glutarate and 4-methylvalerate), the external aldimine model (eBCAT•2-methylleucine), and the true ketimine intermediate (eBCAT•glutamate), the stereochemistry of the reaction process (half-reaction) from glutamate to 2-oxoglutarate is outlined (Figure 7) (*11*). The mechanism for one half-reaction in DAAT has been proposed in terms of three structures (native form, a complex with the reduced analogue of the external aldimine, and a PMP form of bsDAAT) (*9*).

The glutamate substrate approaches the *si*-face of PLP with its α-amino group directed toward the Schiff base of PLP. The α-carboxylate and the side chain of the substrate are located on the phosphate and the O3- sides of PLP, respectively and are recognized as described above. Concurrently, the flexible interdomain loop approaches and encloses the substrate to give the Michaelis complex (Figure 7A). In

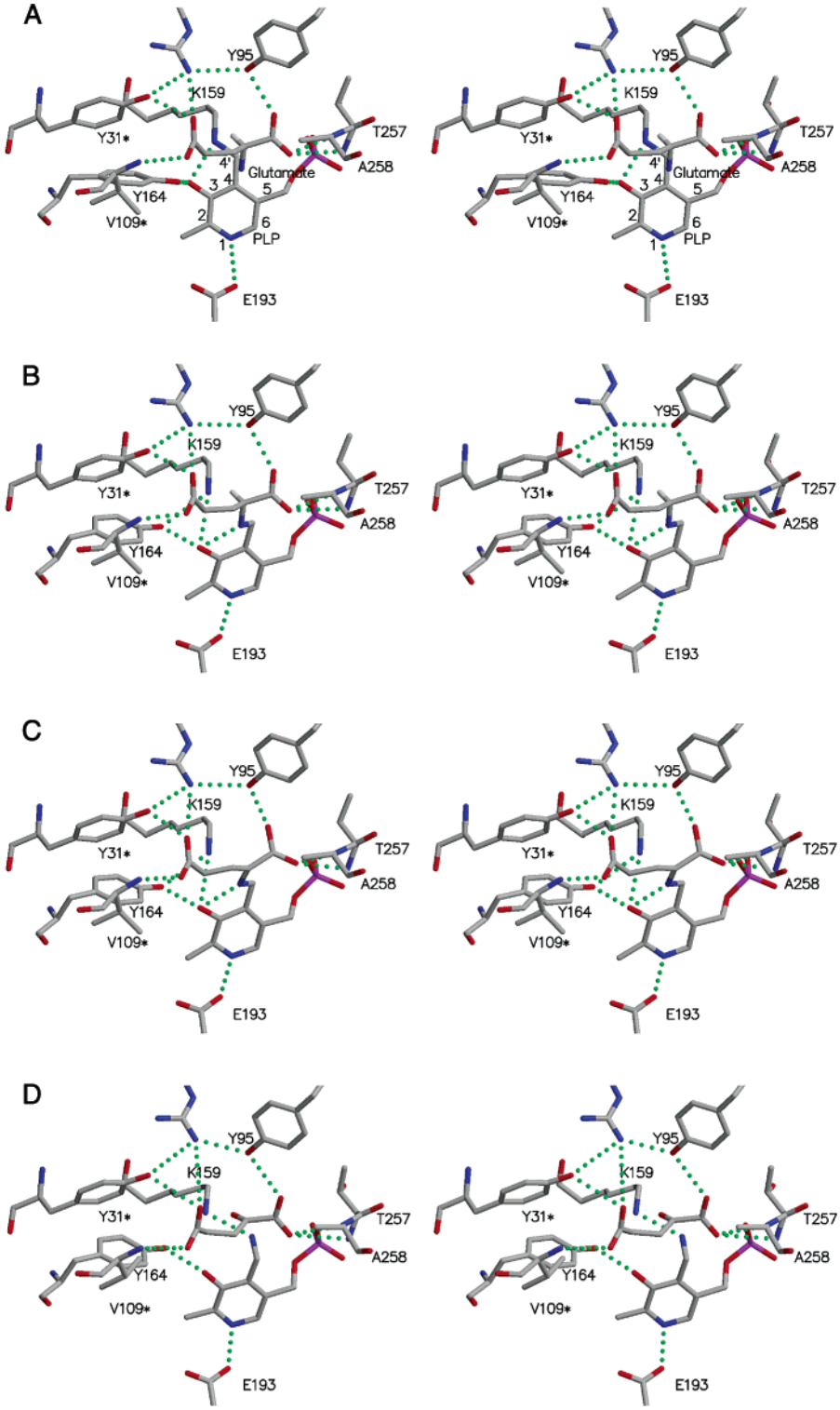

FIGURE 7: Stereoview of catalytic intermediate models of half transamination reaction. Putative hydrogen bonds are shown by dotted lines. (A) Michaelis complex between PLP enzyme and glutamate. The α-hydrogen atom is attached to Cα atom of the substrate. (B) External aldimine (Schiff base between PLP and glutamate). The α-hydrogen atom is attached to Cα atom of the substrate. (C) Ketimine intermediate. (D) Michaelis complex between PMP enzyme and 2-oxoglutarate.

this complex, PLP−Lys159 has essentially the same conformation as that observed in the unliganded form where the Schiff-base bond is coplanar with the pyridine ring of PLP.

The C4′ atom of PLP is activated by the protonation of the Schiff base and undergoes nucleophilic attack by the substrate α-amino group from the *si*-face side. Through the tetrahedral intermediate, a new Schiff (external aldimine) base is formed between PLP and the substrate (Scheme 2 and Figure 7B). The released Lys159 makes hydrogen bonds with Tyr164 and O3- of PLP. Through this process, the bound substrate does not change its location, while PLP rotates its pyridine ring about 30° around the N1−C4 bond of PLP toward the solvent side (*si*-face side). It is reasonable to assume that the cofactor−substrate adducts from the external aldimine to ketimine have nearly the same confor-

mation since the X-ray structure of the external aldimine model is essentially the same as that of the ketimine form. The substrate α-carbon is activated by the protonated Schiff base and the protonated pyridine ring nitrogen. The amino group of the catalytic Lys159 is in a favorable position to shuttle protons to the Cα atom of the substrate and the C4′ of the cofactor: the distances between the amino nitrogen of Lys159 and Cα and C4′ are 4.1 and 3.0 Å and 4.3 and 3.0 Å in eBCAT•glutamate and eBCAT•2-methylleucine, respectively. The deprotonated amino group of Lys159 abstracts an α-proton of the substrate from the *re*-side of the cofactor yielding the quinonoid intermediate (Scheme 2). After α-proton elimination, Lys159 adds a proton to the C4′ atom of the quinonoid intermediate yielding the ketimine intermediate (Figure 7C).

The ketimine intermediate is hydrolyzed to yield 2-oxoglutarate and PMP. A water molecule attacks the Cα atom of the substrate from the *re*-side of the cofactor to form the carbinolamine (Scheme 2), which is cleaved to 2-oxoglutarate and PMP (Figure 7D). Through the entire process shown in Figure 7, the substrate is enclosed in the same surroundings irrespective of whether it is hydrophobic or acidic, and the stereospecificity of the reaction is ensured by the fixing of the α-carboxylate and side chain at their recognition sites. The same reaction process will also apply to hmBCAT (*12*) since the active site structures and most of the active site residues are conserved between eBCAT and hmBCAT. However, the location and conformation of the interdomain loop of eBCAT seems to be different from that of hmBCAT, resulting in the incomplete shielding of the bound substrate from the solvent region (see *Double Substrate Recognition*).

The cofactor of eBCAT belonging to fold type IV directs its *re*-face toward the protein side (*re*-face specificity of the reaction) in contrast to the PLP enzymes of fold types I−III with *si*-face specificity. Consequently, the α-carboxylate of the bound substrate L-amino acid is on the phosphate side of PLP, resulting in a repulsive interaction because of a short contact between the α-carboxylate and the phosphate groups: 3.3, 3.8, 4.2, and 3.5 Å in eBCAT complexes with glutamate, 2-methylleucine, glutarate, and 4-methylvarelate. The repulsive force, which is not favorable for substrate binding, is relaxed if a proton lies between the two negative groups. In the unliganded eBCAT, the internal aldimine bond (Schiff base, C4′ = N4) is coplanar with the PLP ring indicating that the protonated Schiff base is hydrogen-bonded to O3- of PLP. On the approach of the substrate amino acid to the active site, the protonated α-amino group of the substrate comes close to the protonated Schiff base. The α-amino group of the substrate must then be deprotonated to form a new Schiff base with PLP (Scheme 2). The migration of the proton on the α-amino group of the substrate to the short contact pair between the α-carboxylate and the phosphate of PLP would reduce the electrostatic repulsion between the pair and render the α-amino group of the substrate deprotonated.

REFERENCES

1. Christen, P., and Metzler, D. E., Eds. (1985) *Transaminases*, J. Wiley and Sons, New York.
2. Malashkevich, V. N., Onuffer, J. J., Kirsch, J. F., and Jansonius, J. N. (1995) *Nature Struct. Biol. 2*, 548−553.
3. Okamoto, A., Nakai, Y., Hayashi, H., Hirotsu, K., and Kagamiyama, H. (1998) *J. Mol. Biol*. *280*, 443−461.
4. Haruyama, K., Nakai, T., Miyahara, I., Hirotsu, K., Mizuguchi, H., Hayashi, H., and Kagamiyama, H. (2001) *Biochemistry 40*, 4633−4644.
5. Grishin, N. V., Phillips, M. A., and Goldsmith, E. J. (1995) *Protein Sci. 4*, 1291−1304.
6. Jansonius, J. N. (1998) *Curr. Opin. Struct. Biol. 8*, 759−769.
7. Yoshimura, T., Nishumura, K., Ito, J., Esaki, N., Kagamiyama, H., Manning, J. M., and Soda, K. (1993) *J. Am. Chem. Soc*. *115*, 3897−3900.
8. Sugio, S., Petsko, G. A., Manning, J. M., Soda, K., and Ringe, D. (1995) *Biochemistry 34*, 9661−9669.
9. Peisach, D., Chipman, D. M., van Ophem, P. W., Manning, J. M., and Ringe, D. (1998) *Biochemistry 37*, 4958−4967.
10. Okada, K., Hirotsu, K., Sato, M., Hayashi, H., and Kagamiyama, H. (1997) *J. Biochem. 21*, 637−641.
11. Okada, K., Hirotsu, K., Hayashi, H., and Kagamiyama, H. (2001) *Biochemistry 40*, 7453−7563.
12. Yennawar, N., Dunbar, J., Conway, M., Hutson, S., and Farber, G. (2001) *Acta Crystallogr. D 57*, 506−515.
13. Nakai, T., Mizutani, H., Miyahara, I., Hirotsu, K., Takeda, S., Jhee, K. H., Yoshimura, T., and Esaki, N. (2000) *J. Biochem. 128*, 29−38.
14. Jhee, K.-H., Yoshimura, T., Miles, E. W., Takeda, S., Miyahara, I., Hirotsu, K., Soda, K., Kawata, Y., and Esaki, N. (2000) *J. Biochem. 128*, 679−686.
15. Inoue, K., Kuramitsu, S., Aki, K., Watanabe, Y., Takagi, T., Nishigai, M., Ikai, A., and Kagamiyama, H. (1988) *J. Biochem. 104*, 777−784.
16. Karpeisky, M. Y., and Ivanov, V. I. (1966) *Nature 210*, 493−496.
17. Kirsch, J. F., Eichele, G., Ford, G. C., Vincent, M. G., Jansonius, J. N., Gehring, H., and Christen, P. (1984) *J. Mol. Biol. 174*, 497−525.
18. Malashkevich, V. N., Toney, M. D., and Jansonius, J. N. (1993) *Biochemistry 32*, 13451−13462.
19. Otwinowski, Z. (1993) Data collection and processing in *Proceedings of the CCP4 Study Weekend*, pp 56−62, SERC Daresbury Laboratory, Warrington.
20. Jones, T. A., Zou, J.-Y., Cowan, S. W., and Kjeldgaard, M. (1991) *Acta Crystallogr. A 47*, 110−119.
21. Brunger, A. T., Adams, P. D., Clore, G. M., DeLano, W. N., Gros, P., Grosse-Kunstleve, R. W., Jiang, J.-S., Kuszewski, J., Nilges, M., Pannu, N. S., Read, R. J., Rice, L. M., Simonson, T., and Warren, G. L. (1998) *Acta Crystallogr. D 54*, 905−921.
22. Laskowski, R. A., MacArthur, M. W., Moss, D. S., and Thornton, J. M. (1993) *J. Appl. Crystallogr. 26*, 283−291.
23. Kraulis, P. J. (1991) *J. Appl. Crystallogr. 24*, 946−950.
24. Esnouf, R. M. (1997) *J. Mol. Graphics 15*, 132−134.
25. Merritt, E. A., and Bacon, D. J. (1997) *Methods Enzymol. 277*, 505−524.
26. Jansonius, J. N., and Vincent, M. G. (1987) Structural basis for catalysis by aspartate aminotransferase in biological macromolecules and assemblies (Jurnak, F. A., and McPherson, A., Eds.) pp 187−285, J. Wiley and Sons, New York.
27. McPhalen, C. A., Vincent, M. G., and Jansonius, J. N. (1992) *J. Mol. Biol. 225*, 495−517.
28. Malashkevich, V. N., Strokopytov, B. V., Borisov, V. V., Dauter, Z., Wilson, K. S., and Torchinsky, Y. M. (1995) *J. Mol. Biol. 247*, 111−124.
29. Okamoto, A., Higuchi, T., Hirotsu, K., Kuramitsu, S., and Kagamiyama, H. (1994) *J. Biochem. 116*, 95−107.
30. Jäger, J., Moser, M., Sauder, U., and Jansonius. J. N. (1994) *J. Mol. Biol. 239*, 285−305.
31. Miyahara, I., Hirotsu, K., Hayashi, H., and Kagamiyama, H. (1994) *J. Biochem. 116*, 1001−1012.
32. Rhee, S., Silva, M. M., Hyde, C. C., Rogers, P. H., Metzler, C. M., Metzler, D. E., and Arnone, A. (1997) *J. Biol. Chem. 272*, 17293−17302.
33. Shen, B. W., Hennig, M., Hohenester, E., Jansonius, J. N., and Schirmer, T. (1998) *J. Mol. Biol. 277*, 81−102.
34. Shah, S. A., Shen, B. W., and Brunger, A. T. (1997) *Structure 5*, 1067−1075.
35. Tanizawa, K., Masu, Y., Asano, S., Tanaka, H., and Soda, K. (1989) *J. Biol. Chem. 264*, 2445−2449.

BI026722F